Pixel-Level Infrared Thermography Data Enhancement Strategy for Aerospace Carbon Fiber Reinforced Polymer

by Fumin Wang[1,2], Stefano Sfarra[2], Yuan Yao[3], Yi Liu[1*]

[1] *Institute of Process Equipment and Control Engineering, Zhejiang University of Technology, Hangzhou, China*

[2] *Department of Industrial and Information Engineering and Economics, University of L'Aquila, L'Aquila, Italy*

[3] *Department of Chemical Engineering, National Tsing Hua University, Hsinchu, Taiwan*

Abstract

Infrared thermography is suitable for large-area non-destructive testing, but it is affected by non-uniform heating and noise, making it difficult to reliably identify weak thermal anomalies. This paper proposes Long short-term memory Autoencoder Principal Component Thermography (LAPCT) to model the spatiotemporal information of thermal image sequences in an end-to-end manner. This method utilizes the temporal dynamic features of each pixel within the sequence as its core input. By maintaining complete spatial relationships at the pixel level, similar temporal modes of neighbouring pixels can enhance each other, thereby providing spatial contextual support for weak dynamic signals. Simultaneously, low-dimensional temporal features focus on the dynamic trajectory of each single pixel, avoiding interference from irrelevant spatial information. Principal component thermography (PCT) is applied to the reconstructed sequence to extract discriminative features. This method significantly enhances defect characterization and improves contrast-to-noise ratio on aerospace carbon fiber reinforced polymer samples, achieving more robust automatic detection compared to the traditional PCT model.

1. Introduction

Carbon fibre reinforced polymer (CFRP) is widely used in load-bearing aerospace structures because of their low weight, high strength, corrosion resistance and fatigue resistance [1]. However, their multilayered and heterogeneous structure, together with complex service environments, makes them prone to hidden defects such as delamination, debonding, porosity and impact damage. These defects can degrade load-bearing capacity and compromise flight safety. Rapid and reliable non-destructive testing (NDT) is therefore essential. Infrared thermography (IRT) [2-5] offers non-contact, full-field and radiation-free inspection, and is well suited for large-area CFRP assessment. However, conventional IRT relies heavily on manual interpretation or threshold-based segmentation. It is also sensitive to non-uniform heating, thermal diffusion and environmental noise, which may lead to missed detection or false alarms for weak defects.

Machine learning [6-8] has been introduced to improve defect recognition in IRT data by enabling automatic thermal feature extraction and defect enhancement. Although conventional machine learning methods improve IRT performance to some extent, they often depend on handcrafted features or low-dimensional statistical representations. This limits their ability to describe nonlinear spatiotemporal features in high-dimensional thermal image sequences under complex backgrounds.

In recent years, deep learning has emerged as a powerful approach for intelligent infrared image analysis [9-11]. Convolutional neural networks and their variants [12] can learn hierarchical spatial features directly from raw thermal images, showing strong potential for defect recognition and background suppression. However, most existing deep learning methods focus on single-frame or local spatial information. They make limited use of the temporal evolution embedded in infrared thermal sequences. This is a critical limitation because defect responses are dynamic thermal anomalies. Neglecting temporal correlations may weaken the representation of weak or deep defects.

To address these limitations, a long short-term memory autoencoder principal component thermography method, termed LAPCT, is proposed for infrared thermographic defect detection in aerospace CFRP structures. LAPCT combines the long-sequence modelling capability of Long short-term memory (LSTM) networks with the compact representation learning ability of autoencoders. It learns defect-sensitive latent temporal features from infrared thermal sequences in an end-to-end manner. During training, the encoder captures dynamic features from pixel-wise temperature evolution profiles. The decoder then reconstructs the original thermal sequence from the latent representation. This reconstruction suppresses non-uniform background responses and random noise, while enhancing defect-related thermal signatures. Principal component thermography is subsequently applied to the reconstructed data to extract more discriminative features, thereby improving defect visibility and detection reliability. The proposed method is finally validated on a real aerospace composite specimen, and its performance is quantitatively assessed using the contrast-to-noise ratio (CNR).

2. Data Acquisition

Pulsed thermography (PT) is a widely used modality of active IRT. In this approach, a short-duration, high-energy thermal pulse is applied as an external excitation to induce a transient temperature perturbation on the inspected surface, rather than imposing a continuous thermal load. The experimental system is shown in Figure 1. Compared with continuous heating, pulsed excitation establishes a well-defined initial thermal state over a short timescale and provides clearer boundary characteristics for the subsequent heat-diffusion process. It also typically yields higher thermal contrast and signal-to-noise ratio, thereby reducing the influence of fluctuations in the ambient background on the measurements. As the thermal diffusion length increases with time, the early post-pulse temperature response is governed primarily by near-surface heat conduction, making PT particularly sensitive to shallow subsurface defects and capable of resolving them with high spatial precision.

Figure 1. Experimental data acquisition equipment

During PT data acquisition, an infrared camera continuously records the transient thermal response of the specimen at a prescribed frame rate f over an acquisition period of n s. The resulting thermal video is then decomposed frame by frame to generate p infrared thermograms. To minimize the influence of non-informative temporal segments on subsequent analysis, background frames acquired before thermal excitation and redundant frames recorded after the specimen has returned to a stable cooling state are removed. This preprocessing yields N effective thermal-response images, each with a spatial resolution of $N_x \times N_y$. The effective image sequence is subsequently stacked in chronological order, and the two-dimensional spatial pixels of each frame are unfolded into a one-dimensional vector. This procedure constructs a two-dimensional thermal-response matrix with dimensions $N \times (N_x N_y)$. It fully preserves the information regarding the temporal evolution of the temperature field and serves as the foundational input for subsequent feature extraction and model analysis.

To improve numerical stability and accelerate convergence during model training, the two-dimensional thermal-response matrix is subjected to Min–Max normalization before being introduced into the model. This operation maps the original temperature responses onto a unified numerical scale, reducing the influence of amplitude variations among different pixels or samples on the optimization process. The normalization is expressed as:

$$X_{\text{norm}} = \frac{X - X_{\min}}{X_{\max} - X_{\min}} \tag{1}$$

where X denotes the original thermal-response matrix, and $X_{\min}$ and $X_{\max}$ represent the minimum and maximum values along the corresponding normalization dimension, respectively. X_{norm} denotes the normalized input matrix used for model training.

3. Long-Short-Term Memory Autoencoder Thermography

In infrared thermography, thermal-response sequences generally contain both defect-induced dynamic signatures and redundant components arising from environmental perturbations, material heterogeneity, and imaging noise. LSTM networks provide an effective framework for modelling such temporal thermal image sequences through a gated state-updating mechanism. Their principal advantage lies in the selective retention, renewal, and suppression of information across successive time steps, enabling the capture of physically meaningful long-range dependencies during the evolution of infrared thermal fields.

Specifically, the input gate regulates the extent to which thermal-response information at the current time step is written into the cell state, allowing the network to preferentially incorporate discriminative features associated with defect-induced thermal anomalies. The forget gate adaptively determines the proportion of historical information to be retained based on the current input and the previous memory state, thereby attenuating the influence of outdated, repetitive, or noise-dominated thermal components on subsequent inference. The output gate further governs which information encoded in the cell state is projected into the current hidden representation, enabling the model to extract effective features closely related to transient heat-diffusion behaviour at each frame. Through the coordinated

operation of these three gating units, the LSTM can jointly characterise the spatial distribution and temporal evolution of thermal images in IRT sequence analysis, thereby improving the fidelity of defect-region representation and enhancing the stability and robustness of the detection process. Therefore, this study proposes a novel LAPCT model for data enhancement in IRT. Given that temporal correlations among thermal image frames play a critical role in defect characterization and recognition, LAPCT is designed to systematically exploit the temporal dependencies embedded in consecutive thermal-response frames and to extract latent spatiotemporal representations. By integrating LAPCT with thermal image data, the proposed model preserves the spatial information contained in individual frames while effectively capturing the dynamic evolution of thermal responses across image sequences. This enables a more informative representation of defect-related features and consequently improves detection accuracy. The overall architecture of the proposed model is illustrated in Figure 2.

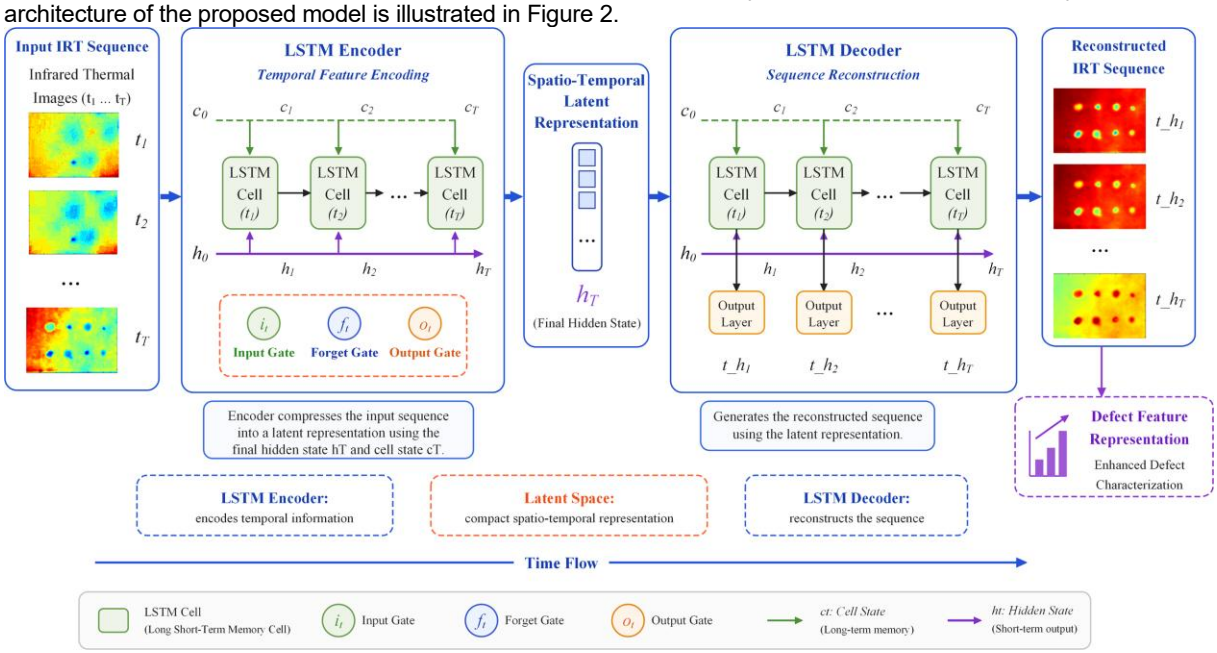

Figure 2. Schematic Diagram of the LAPCT Model

The proposed model follows a sequence-to-sequence autoencoder architecture consisting of an encoder and a decoder. Given an infrared thermography sequence $\{\mathbf{x}_t\}_{t=1}^{N}$, the encoder recursively updates the hidden and cell states through stacked LSTM units, thereby extracting temporal dependencies from consecutive thermal responses and compressing them into a compact latent representation. The decoder then uses the encoded temporal features to reconstruct the thermal representation at each time step, while a fully connected layer projects the decoder state back to the original feature space. The process is formulated as:

$$(\mathbf{h}_t^{\text{enc}}, \mathbf{c}_t^{\text{enc}}) = \text{LSTM}_{\text{enc}}\left(\mathbf{x}_t, \mathbf{h}_{t-1}^{\text{enc}}, \mathbf{c}_{t-1}^{\text{enc}}\right) \tag{2}$$

$$(\mathbf{h}_t^{\text{dec}}, \mathbf{c}_t^{\text{dec}}) = \text{LSTM}_{\text{dec}}\left(\mathbf{z}_t, \mathbf{h}_{t-1}^{\text{dec}}, \mathbf{c}_{t-1}^{\text{dec}}\right), \quad \mathbf{z}_t = \mathbf{h}_t^{\text{enc}} \tag{3}$$

$$\mathbf{x}_t = \text{FC}\left(\mathbf{h}_t^{\text{dec}}\right) = \mathbf{W}_o \mathbf{h}_t^{\text{dec}} + \mathbf{b}_o \tag{4}$$

where $\mathbf{x}_t$ denotes the input thermal feature at time step t; $\mathbf{h}_t^{\text{enc}}$ and $\mathbf{c}_t^{\text{enc}}$ are the hidden and cell states of the encoder, respectively; $\mathbf{h}_t^{\text{dec}}$ and $\mathbf{c}_t^{\text{dec}}$ are the corresponding decoder states; $\mathbf{z}_t$ represents the latent temporal feature passed to the decoder; $\mathbf{x}_t$ is the reconstructed output; and $\mathbf{W}_o$ and $\mathbf{b}_o$ are the weight matrix and bias term of the output projection layer.

Within this framework, the encoder exploits the temporal modelling capability of LSTM to learn dynamic correlations among successive thermal frames and to condense defect-related thermal responses into a low-dimensional representation. The decoder reconstructs the frame-wise thermal features under the constraint of this latent representation, allowing the reconstructed sequence to remain consistent with the original data in both spatial distribution and temporal evolution. Because the reconstructed sequence retains the same number of frames as the original input, principal component thermography is subsequently applied to reduce data redundancy. The first M principal components are retained and visualised to obtain M principal-component thermograms for defect analysis. The first M principal components are retained and visualised to obtain M principal-component thermograms for defect analysis.

4. Experiment

In this section, the proposed LAPCT-based data enhancement method is applied to defect detection in honeycomb sandwich carbon-fibre composite panels. To quantitatively evaluate the enhancement of defect-related thermal responses, the contrast-to-noise ratio (CNR) is adopted as the evaluation metric. CNR measures the detectability of the thermal-response difference between the defective region and the defect-free reference region relative to background noise fluctuations, and is defined as:

$$\mathrm{CNR} = \frac{|\mu_{\mathrm{d}} - \mu_{\mathrm{b}}|}{\sigma_{\mathrm{b}}} \tag{5}$$

where μ_{d} denotes the mean pixel intensity of the defective region in the thermal image, μ_{b} denotes the mean pixel intensity of the defect-free background region, and σ_{b} is the standard deviation of the pixel intensities in the defect-free background region. CNR characterizes the separability of the defect response from the background noise. A higher CNR value indicates a more pronounced contrast between the defective and background regions, demonstrating that the method can more effectively enhance defect-related features and improve defect detectability.

4.1. CFRP Specimen and Data Collection

In this study, experiments were performed on a honeycomb sandwich carbon-fibre-reinforced polymer (CFRP) specimen representative of panels used in aircraft cargo-compartment sidewalls and flooring structures. The specimen contained a honeycomb core. To reproduce leakage scenarios that may occur in in-service components, through-holes with different diameters were introduced on the rear surface of the specimen and alternately filled with water and aviation oil in a crossed arrangement, thereby simulating water and oil leakage defects. The specimen measured 24.5cm×15.8cm×1.0cm, and the hole diameters were 1.3 cm, 1.0 cm, 0.8 cm and 0.7 cm, as shown in Figure 3.

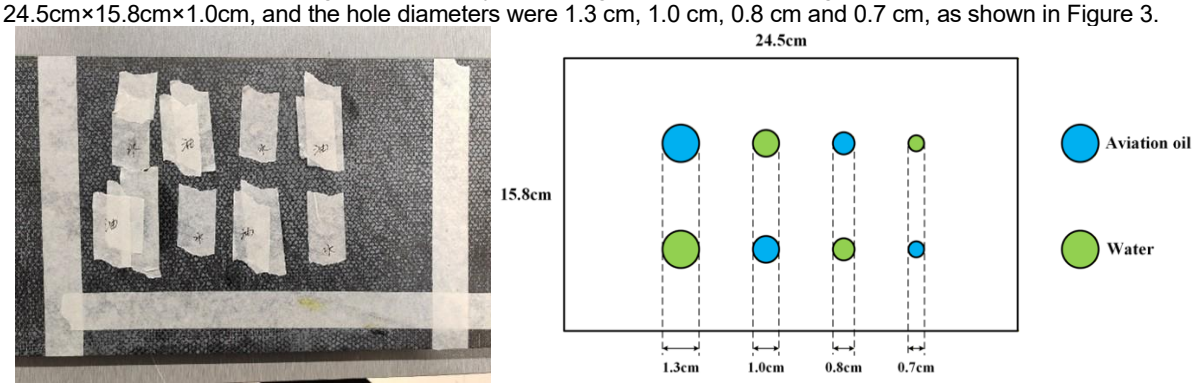

Figure 3. Distribution of Sample Defects

Data acquisition was conducted using the pulsed thermography (PT) system shown in Fig. 1. Transient thermal excitation was applied at the maximum output power of two Golden Eagle flash lamps, after which the cooling process was recorded from the intact surface using a DL-700 infrared camera at an actual frame rate of 12 fps for 13 s. The recorded video was decomposed into 157 thermal images with a spatial resolution of 640×480 pixels. After removing frames acquired before heating and after complete cooling, and after cropping the region of interest (ROI), 55 thermal images with a resolution of 210×295 pixels were retained for subsequent analysis.

Figure 4 presents the raw thermal images of the specimen recorded at different observation times, with two representative frames selected from the early, intermediate and late stages of the acquisition sequence. The colour scale adjacent to each image denotes the corresponding pixel-intensity distribution within the imaged region. Immediately after the termination of thermal excitation, the subsurface damage does not yet generate sufficient thermal contrast to be clearly distinguished. As cooling proceeds, local thermal anomalies associated with the defective regions gradually emerge, owing to differences in heat diffusion and thermal conduction between damaged and intact areas. Nevertheless, the visibility of these features remains limited by non-uniform background responses and residual noise in the raw thermograms. Accordingly, direct interpretation of the unprocessed thermal images is insufficient for robust defect identification, highlighting the need for reliable temporal-analysis and contrast-enhancement methods to improve detection sensitivity and accuracy.

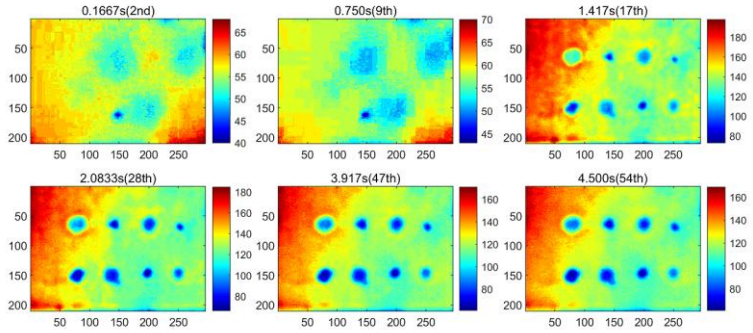

Figure 4. Thermal images of CFRP specimens acquired at different time points

4.2. Discussion of experimental results

To verify the applicability and effectiveness of the proposed LAPCT method, it was applied to the honeycomb sandwich carbon-fibre-reinforced polymer composite specimen for experimental evaluation. Representative visual results are shown in Figure 5. Compared with the raw thermal images, the LAPCT-enhanced early-stage sequences reveal the defect-related linear features with greater clarity. Meanwhile, the spatially non-uniform background is effectively suppressed, and the thermal contrast between defective and sound regions is markedly improved, thereby enhancing the detectability of subsurface defects. However, because the enhancement procedure does not reduce the number of frames in the image sequence, frame-by-frame inspection still involves considerable computational and interpretative effort. Therefore, dimensionality reduction is further required to compress redundant temporal information, reduce the complexity of defect identification, and improve the efficiency and robustness of subsequent analysis.

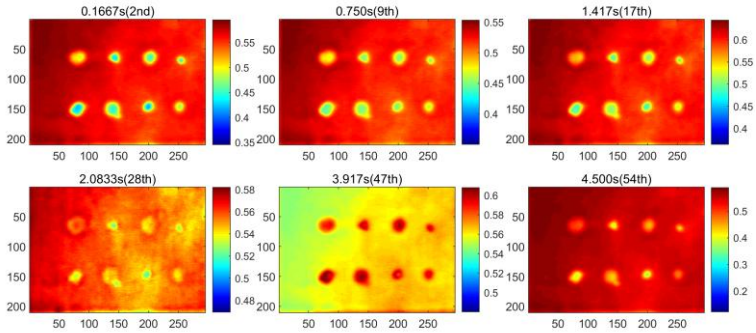

Figure 5. LAPCT-enhanced thermal images of the CFRP specimen at different time points

To further compress the thermal image sequence and improve the practicality of subsequent quantitative analysis, principal component thermography (PCT) was introduced to obtain low-dimensional representations of different processed datasets. To evaluate the effectiveness of the proposed method, PCT was applied to the raw thermal images, convolutional autoencoder principal component thermography (CPCT) [13,14], and LAPCT, respectively. The corresponding results are shown in Figure 6.

Figure 6(a) presents the principal component results obtained from the raw thermal image sequence using PCT. The eight internal defects can be partially represented in the principal component images; however, the results are still strongly affected by non-uniform background interference. In particular, the second principal component (PC2) contains pronounced noise components, which may weaken the stability of subsequent defect identification and quantitative evaluation.

Figure 6(b) shows the results obtained by CPCT. Compared with the PCT results of the raw images, CPCT markedly suppresses random noise, leading to a smoother grey-level distribution in the non-defective regions. Meanwhile, the contrast between the defective regions and the background is enhanced in the third principal component (PC3). Nevertheless, the background non-uniformity is not completely removed. This limitation is mainly attributed to the fact that the convolutional autoencoder-based enhancement primarily improves the overall spatial intensity distribution but cannot fully distinguish defect-related responses from background variations and noise components. Consequently, while the defect signals are enhanced, residual background fluctuations and noise may also be amplified to some extent.

In contrast, the LAPCT results shown in Figure 6(c) exhibit superior defect representation capability. The proposed method effectively suppresses the influence of non-uniform background on the principal component results and substantially improves the grey-level contrast between the defect regions and the surrounding matrix. Visual inspection demonstrates that LAPCT preserves defect-related temporal features while more effectively attenuating background fluctuations and noise interference, thereby producing clearer and more stable defect-response images. These results indicate that the data enhancement component of LAPCT enhances defect-related temporal features and suppresses

background noise, while the subsequent PCT step reduces data redundancy and extracts more discriminative principal component heatmaps.

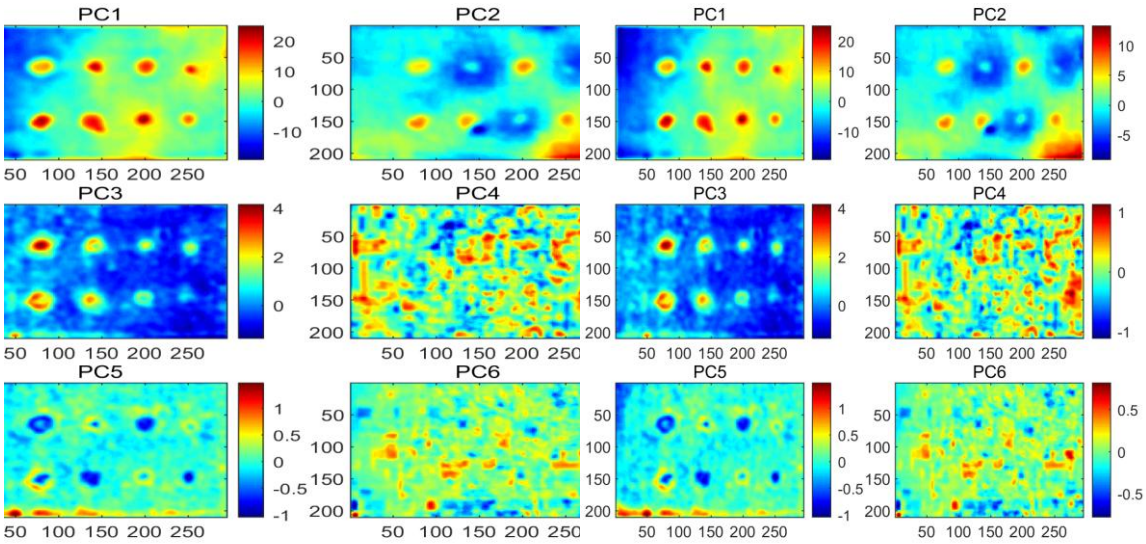

(a)PCT (b) CPCT

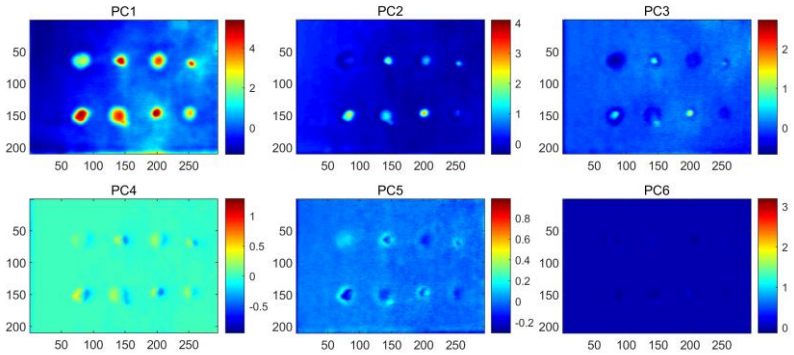

(c) LAPCT

Figure 6. Analytical results of different methods: (a) PCT, (c) CPCT, (c) LAPCT

To further verify the reliability of the visual observations, the contrast-to-noise ratio (CNR) was used to quantitatively evaluate the defect-enhancement performance of different methods. Table 1 summarizes the peak CNR values obtained at each defect location. Overall, the variation in CNR is highly consistent with the visual interpretation of the thermal images, confirming that the quantitative assessment supports the conclusions drawn from the image-based analysis.

Table 1. Comparative CNR results of three methods analyses

Methods	CNR							
	D1	D2	D3	D4	D5	D6	D7	D8
PCT	4.486	2.889	2.371	2.381	4.256	3.279	2.753	2.133
CPCT	**5.068**	3.308	2.755	2.516	**4.725**	3.707	2.716	2.663
LAPCT	4.045	**3.801**	**4.876**	**4.147**	4.490	**5.424**	**5.207**	**3.900**

Compared with the PCT and CPCT results, LAPCT improves the CNR at all defect locations to varying degrees, with the most pronounced enhancement observed for the small defects on the right side. This indicates that LAPCT is more effective in extracting weak defect responses and highlighting local anomalies under non-uniform background conditions. Although CAT yields higher CNR values at D1 and D5, the grey-level difference between the defect boundaries and the surrounding background remains limited. As a result, these regions are still susceptible to background fluctuations, which may reduce the practical separability of the defects.

In summary, the visual results and CNR-based evaluation demonstrate that LAPCT provides more stable enhancement and stronger robustness against background interference for most defects. These findings suggest that LAPCT can effectively enhance defect contrast while suppressing the effects of non-uniform backgrounds and noise.

5. Conclusion

In this study, a LAPCT method is proposed to improve the visualization of defect features in infrared thermal images of honeycomb sandwich carbon-fibre-reinforced polymer composites. By exploiting the inter-frame correlations within the thermal image sequence, the method adaptively smooths and suppresses interfering components, such as noise fluctuations and spatially non-uniform background responses. As a result, early-stage thermal response features are enhanced, while the contrast between defective and sound regions is markedly improved. The data enhancement module of LAPCT first reconstructs and enhances thermal sequences by leveraging inter-frame correlations and then combines this with PCT to compress the enhanced sequences and extract compact, defect-sensitive features. This strategy not only lowers the complexity of frame-by-frame inspection but also improves the efficiency and stability of defect detection. Finally, the proposed method is experimentally validated on a practical aircraft cargo-panel honeycomb sandwich structure under simulated water- and oil-leakage conditions, and its enhancement capability and detection effectiveness are quantitatively evaluated using the contrast-to-noise ratio (CNR).

Acknowledgements

Yi Liu was supported in part by the National Natural Science Foundation of China (Grant No. U23A20328). Yuan Yao was supported in part by the National Science and Technology Council, Taiwan, under Project NSTC 114-2218-E-007-018.

References

[1] Popow V, Vogtmann J, Gurka M. In-situ characterization of impact damage in carbon fibre reinforced polymers using infrared thermography[J]. Infrared Physics & Technology, 2022, 122: 104074.

[2] Liu Y, Yao Y, Wang F, et al. Review of unsupervised machine learning methods in active infrared thermography for defect detection and analysis[J]. Quantitative InfraRed Thermography Journal, 2025: 1–28. Doi: 10.1080/17686733.2025.2540662.

[3] Sfarra S, Tejedor B, Perilli S, et al. Evaluating the freeze–thaw phenomenon in sandwich-structured composites via numerical simulations and infrared thermography[J]. Journal of Thermal Analysis and Calorimetry, 2021, 145(6): 3105–3123.

[4] Li S, Han S, Wang J, et al. Infrared thermography detection of grouting defects in external post-tensioned tendon ducts under construction hydration heat excitation[J]. NDT & E International, 2023, 134: 102785.

[5] Zhou G, Ong Z C, Zhang Z, et al. Defect detection of carbon fiber deflectors based on laser infrared thermography and experimental modal analysis[J]. Mechanical Systems and Signal Processing, 2024, 221: 111763.

[6] Yousefi B, Sfarra S, Sarasini F, et al. Low-rank sparse principal component thermography (sparse-PCT): Comparative assessment on detection of subsurface defects[J]. Infrared Physics & Technology, 2019, 98: 278-284.

[7] Oswald-Tranta B. Time and frequency behaviour in TSR and PPT evaluation for flash thermography[J]. Quantitative InfraRed Thermography Journal, 2017, 14(2): 164–184.

[8] Liu M, Liu T, Liu B, et al. Defect detection in CFRP combining SK-means clustering and probability of detection analysis[J]. Quantitative InfraRed Thermography Journal, 2026, 23(1): 40–52.

[9] Deng L, Zuo H, Wang W, et al. Internal defect detection of structures based on infrared thermography and deep learning[J]. KSCE Journal of Civil Engineering, 2023, 27(3): 1136-1149.

[10] Cheng L, Tong Z, Xie S, et al. IRT-GAN: A generative adversarial network with a multi-headed fusion strategy for automated defect detection in composites using infrared thermography[J]. Composite Structures, 2022, 290: 115543.

[11] Khatri A, Khadka S, Lamichhane N, et al. A comprehensive review of infrared thermography and deep learning applications for solar photovoltaic systems[J]. Infrared Physics & Technology, 2025, 148: 105878.

[12] Bu C, Shen R, Bai W, et al. CNN-based defect detection and classification of PV cells by infrared thermography method[J]. Nondestructive Testing and Evaluation, 2025, 40(5): 1752–1769.

[13] Liu Y, Wang F, Liu K, et al. Deep convolutional autoencoder thermography for artwork defect detection[J]. Quantitative InfraRed Thermography Journal, 2024, 21(6): 367–383.

[14] Yerneni N P, Sainath L, Ghali V S, et al. Automatic Deep Anomaly Detection using Thermography based Convolution Autoencoder Framework[J]. Journal of Nondestructive Evaluation, 2026, 45(2): 66.